Title

Characterizing the interplay of Pauli repulsion, electrostatics, dispersion and charge transfer in halogen bonding with energy decomposition analysis.

Journal

Physical chemistry chemical physics : PCCP, 20(2)

ISSN

1463-9076

Authors

Thirman, Jonathan
Engelage, Elric
Huber, Stefan M
et al.

Publication Date

2018

DOI

10.1039/c7cp06959f

Peer reviewed

Journal Name

ARTICLE TYPE

Cite this: DOI: 10.1039/xxxxxxxxxx

Characterizing the Interplay of Pauli Repulsion, Electrostatics, Dispersion and Charge Transfer in Halogen Bonding with Energy Decomposition Analysis

Jonathan Thirman,*[a], Elric Engelage[b], Stefan M. Huber[b], and Martin Head-Gordon*[c]

Received Date
Accepted Date

DOI: 10.1039/xxxxxxxxxx

www.rsc.org/journalname

The halogen bond is a class of non-covalent interaction that has attracted considerable attention recently. A widespread theory for describing them is the σ-hole concept, which predicts that the strength of the interaction is proportional to the size of the σ-hole, a region of positive electrostatic potential opposite a σ bond. Previous work shows that in the case of CX_3I, with X equal to F, Cl, Br, and I, the σ-hole trend is exactly opposite to the trend in binding energy with common electron pair donors. Using energy decomposition analysis (EDA) applied to a potential energy scan as well as the recent adiabatic EDA technique, we show that the observed trend is a result of charge transfer. Therefore a picture of the halogen bond that excludes charge transfer cannot be complete, and permanent and induced electrostatics do not always provide the dominant stabilizing contributions to halogen bonds. Overall, three universally attractive factors, polarization, dispersion and charge transfer, together with permanent electrostatics, which is usually attractive, drive halogen bonding, against Pauli repulsion.

1 Introduction

Non-covalent interactions have been the subject of considerable theoretical interest in recent years for their importance in a wide variety of molecular systems[1,2]. One such interaction is halogen bonding, which has been known for a long time[3], and has assumed increasing importance and visibility over the past decade or two[4–7]. Halogen bonding is a contributor to supramolecular interactions in the solid state[6–8], and in solution[7,9], and thus is a controllable factor in molecular recognition[10]. Halogen bonding is therefore also significant in biomolecular and medicinal chemistry[11]. As defined by IUPAC[12], "a halogen bond occurs when there is evidence of a net attractive interaction between an electrophilic region associated with a halogen atom (X) in a molecular entity and a nucleophilic region (B) in another, or the same, molecular entity." A halogen bond has the general form $R-X\cdots B$, where the XB distance is less than Van der Waals separation, $\angle RXB \approx 180°$, and the RX bond-length is slightly elonganted. As it is a Lewis acid (X) - Lewis base (B) interaction, it is not surprising that halogen bonding can also affect chemical reactivity.[13]

There has been much effort to characterize the nature of the halogen bond, beyond the overall energetic and structural characteristics given above. It is fair to say that there is no broadly accepted consensus today. Let us begin with IUPAC[12], who suggest that "the forces involved in the formation of the halogen bond are primarily electrostatic". However, they immediately add a cautionary note: "but polarization, charge transfer, and dispersion contributions all play an important role. The relative roles of the different forces may vary from one case to the other." The origin of this slightly tortured statement can be traced to literature controversy. The halogen bond was traditionally considered to be a type of charge transfer complex[14,15], analogous to a hydrogen bond but with a halogen rather than hydrogen atom as the electron pair acceptor. A key role for charge transfer has also been supported by some more recent work[16–26]. However, another recent line of thinking, reflected in the IUPAC definition, describes halogen bonding as being controlled by electrostatics[27–35]. Others have noted roles for dispersion[36] and exchange-repulsion[37], as well as electrostatics.

Supporters of the electrostatics-is-primary approach point to importance of the σ-hole concept[27], which has been applied to a wide variety of non-covalent interactions[30,35]. Proponents of the σ-hole believe in the importance of electrostatic phenomena in explaining non-covalent interactions at the expense of charge transfer, with similar theories in cases such as hydrogen bonding[38]. Some have doubted the validity of the concept of charge

[a] Kenneth S. Pitzer Center for Theoretical Chemistry, Department of Chemistry, University of California, Berkeley, Berkeley, California 94720, United States; E-mail: thirman@berkeley.edu
[b] Organische Chemie I, Fakultät für Chemie und Biochemie, Ruhr-Universität Bochum, Universitätsstraße 150, D-44801 Bochum, Germany; E-mail: stefan.m.huber@rub.de
[c] Kenneth S. Pitzer Center for Theoretical Chemistry, Department of Chemistry, University of California, Berkeley, Berkeley, California 94720, United States; E-mail: mhg@cchem.berkeley.edu

transfer[33,34], viewing it as a misunderstanding of polarization.

What, then, is the physical content of the σ-hole picture? The σ-hole is defined as an area of positive electrostatic potential near an atom and is intended as a measure of its strength as an electron pair acceptor. The electrostatic potential of a molecule is computed on an electron density isosurface – traditionally at the arbitrary value of 0.001 electrons per cubic Bohr radius. When the molecule has electronegative substituents, there is generally a positive potential on this surface at the point opposite the σ bond between the acceptor halogen atom and the central atom, as illustrated for CF_3I in Figure 1. The σ-hole picture states that the halogen bond is an electrostatic interaction between the area of positive potential on the acceptor and the negative potential of the donor. This is intended as an explanation for why C–X···B interactions are linear. Meanwhile, halogen atoms can also act as electron pair donors in C–X···H–A hydrogen bonds, with the explanation that the interaction is with the region of more negative potential on the halogen atom along the line half way in between the bond and the σ-hole. Looking for the σ-hole on hydrogen atoms participating in hydrogen bonds finds that the entire atom is of positive potential, which is put forward as an explanation for why hydrogen bonds are often bent rather than linear.

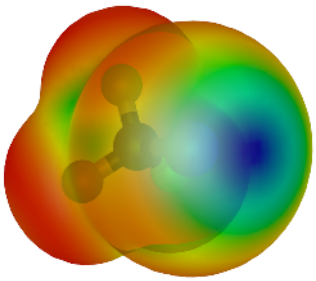

Fig. 1 A plot showing the σ-hole in CF_3I, where the electrostatic potential (ESP) is plotted on an 0.001 au density isosurface. The blue region on the extension of the C−I bond is the positive ESP (favorable for a negative test charge), that represents the σ-hole, while red regions are negative ESP (favorable for a positive test charge).

A charge transfer based explanation of the linearity of halogen bonds would instead describe the interaction as donation from the donor lone pair into the σ* antibonding orbital. This orbital has its highest value in-line with the bond, but in the region beyond both of the bonded atoms, which is to say that the accessible lobe of the σ* orbital is in the same place as the σ-hole. Furthermore, a halogen atom acting as an electron pair donor would donate from a lone pair orbital, which are centered somewhere between the bond and the point opposite — the same place as the region of negative potential. Proponents of the charge transfer picture would argue that donation into the σ* orbital would tend to lengthen, weaken, and red-shift the bond, all of which are experimentally observed in halogen bonds. The σ-hole response to this objection would be that these observations are the result of polarization in response to the presence of the donor[34,39–41]. Because of this consideration, some advocate calculating the σ-hole in the presence of a point charge when the donor is an anion, in order to account for polarization — originally for hydrogen bonds[42], though it has also been proposed for halogen bonds[16].

One of the major arguments deployed in favor of the σ-hole explanation is that the strength of interactions tend to correlate linearly with the size of the σ-hole[29,43–45]. This has been the trend in several different sets of related molecules. This is often taken as proof for the key importance of the σ-hole in understanding halogen bonding. But there is almost necessarily a high level of concordance between the electrostatic and charge transfer pictures as they both attempt to describe the same phenomena. The σ-hole and the lobe of the σ* orbital are in the same place because most the local electron density is concentrated in the σ orbital, and the two orbitals must be orthogonal. There is high electrostatic potential between the bond and the σ-hole in the same place as the lone pair orbitals because the electrons are in the non-bonded orbitals. Polarization and charge transfer leading to similar behavior in the σ bond is not surprising because both are favorable in the same situations. And the correlation of the binding energy with the σ-hole strength may be because of electrostatics, but that does not mean that electrostatics plays the sole role in the interaction. Even in a charge transfer picture, electrostatic effects are also important in hydrogen and halogen bonds. While the bonds are not always perfectly in the direction of the dipole moments, there are usually close and are almost never observed opposing the dipole moments (and when they are, it is in large molecules with far away dipoles — the local electrostatics are still favorable). In addition to a purely electrostatic explanation, this arrangement also makes charge transfer more favorable, as it allows the charge density to move to an area of more positive potential.

The σ-hole may be a good proxy for the overall classical electrostatic interaction — it is a simpler alternative to considering every multipole moment of the two molecules. In large molecules, lower moments give more information about the whole molecule. Information about the local electrostatics is contained in the higher moments, but in a way that is opaque to understanding. Part of the value may come from providing a good descriptor for the local electrostatic environment in complicated systems. But that doesn't make it a unique or uniquely good parameter. In small, symmetrical molecules like the ones that will be discussed here, the dipole moment should be a very reasonable alternative electrostatic parameter. The question is then whether this is enough, or whether the σ-hole can only explain electrostatics, and it is also necessary to consider strength of charge transfer in cases where the two are not correlated (though there is good reason to think that they usually will be).

Recent work by Stefan Huber and colleagues demonstrate a simple family of halogen bond complexes where the trend in binding strength is exactly opposite the trend in σ-hole size[16]. With an acceptor molecule of CX_3I (where X is any of F, Cl, Br, and I) and donors as a halide ion or trimethylamine molecule, iodine as a substituent leads to the strongest interaction, and fluorine the weakest in the order of the periodic table. Of course, the electronegativity trend in halogens goes the opposite direction. This makes CF_3I have the strongest favorable dipole moment, while CI_4 has no dipole at all. The σ-hole trend is the same as the electronegativity one. That means both measures of electrostatics

predict the opposite of the observed trend. This remains the case when varying the halide donor or when changing the acceptor atom from I to Br or Cl.

The most straightforward explanation is that CI_4 is the strongest charge acceptor and that this is enough to overcome the more favorable permanent electrostatic properties of CF_3I. They propose the explanation that CI_4 has the lowest energy σ^* orbital, which allows for stronger charge transfer (according to a charge donation point of view, the interaction strength should go up with $|\langle\sigma^*|H|\mathrm{n}\rangle|^2$ and go down with $E_{\sigma^*} - E_\mathrm{n}$. The limit is $\frac{|\langle\sigma^*|H|\mathrm{n}\rangle|^2}{E_{\sigma^*}-E_\mathrm{n}}$ when the denominator is large compared to the numerator). A schematic view of the charge transfer picture is shown in Figure 2, with a complementary occupied-virtual pair[46] showing the respective orbitals that change is donated from and to. If this point of view is accepted it seems a perspective must be taken that is richer than σ-hole allows, where electrostatics and charge transfer must be considered as separate forces at play in non-covalent interactions. In this work, we will examine some of these systems more closely using energy decomposition analysis to determine the significance of charge transfer in the picture of halogen bonding.

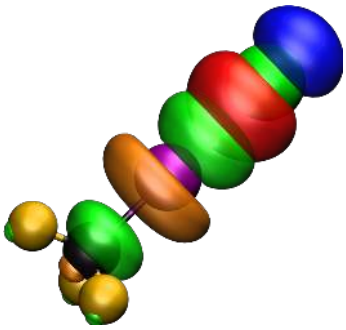

Fig. 2 A complementary occupied-virtual pair[46] for the halogen bond in $CF_3I\cdots Cl^-$. The blue and red represent the positive and negative lobes of a polarized (donor) p orbital on Cl^- and the orange and green represent the positive and negative lobes of a C−I σ^* (acceptor) orbital on CF_3I.

2 Energy decomposition analysis

To resolve the question of whether or not charge-transfer (CT) is a significant contributor to the halogen bond, one needs approaches that can agnostically partition the intermolecular interaction energy into additive contributions that correspond to the relevant physical contributions. These contributions are those that operate in the long-distance regime: specifically permanent and induced electrostatics, and dispersion. In addition Pauli repulsion and CT become relevant as the fragments come close. Energy decomposition analysis (EDA) methods take up this challenge. This area requires reviews to cover in detail, and there are many for this purpose[47–52]. EDA methods should be contrasted with the σ-hole picture: the latter is a picture that does not yield energy contributions at all.

While EDA is in principle the perfect tool to assess the role of CT, there is a catch, however, in that the resulting contributions are not uniquely defined. Accordingly, there are many different EDAs with different strengths and weaknesses. In particular, CT from a given EDA method may be roughly right (the ideal case), or possibly much too large, or conceivably much too small. In either of the latter two cases, misleading results are likely. This is not an idle concern. The widely used natural bond orbital (NBO) analysis[47,53] is known to yield CT contributions that are much too large[54,55], which leads to false conclusions[56–59] about the *absolute* importance of CT (although *relative* NBO CT can be useful as a descriptor[60]). On the other hand, constrained density functional theory[61], which attempts to prevent CT by enforcing constant fragment populations, yields exactly zero CT for symmetric systems such as the double hydrogen bond in the formic acid dimer, a value that is much too small.

Is it possible to usefully proceed, given the reality that CT cannot be uniquely defined? The answer is yes, with one condition. If we wish to assess the role of CT, then we must be reasonably confident that the EDA used does not greatly overestimate, or greatly underestimate CT. Ideally we should have upper and lower bounds for CT contributions, as have been obtained for the water dimer[62]. For this work, we will use a method whose CT contribution has a magnitude that is a *lower bound* to true CT. This way we can be sure that our conclusions regarding CT are conservative. At the same time, the bound is not so weak as to be useless (i.e. we expect our conclusions to be reliable).

For this purpose we use variational energy decomposition analysis[46,63] based on absolutely localized molecular orbitals (ALMOs).[64,65] The ALMO-EDA is a descendant of widely used early EDAs,[66,67] which, like its cousin, the block-localized wavefunction (BLW) EDA[68,69], separates polarization from CT. While originally developed at the mean-field level, the ALMO-EDA was extended by two of us to include electron correlation through second order Møller-Plesset perturbation theory (MP2).[70,71]. The $\mathrm{R-X\cdots B}$ intermolecular interaction energy is decomposed as:

$$\Delta E = \Delta E_\mathrm{frz} + \Delta E_\mathrm{pol} + \Delta E_\mathrm{disp} + \Delta E_\mathrm{CT} \quad (1)$$

The above terms are evaluated from 5 intermediate energies: (i) isolated fragment MP2 energies of $\mathrm{R-X}$ and B (ii) $\mathrm{R-X\cdots B}$ using frozen fragment orbitals and fragment-only correlation amplitudes in the MP2 Hylleraas functional with an orbital relaxation correction (iii) polarized ALMOs and relaxed fragment-only amplitudes (iv) polarized ALMOs and fragment plus dispersive amplitudes, and (v) the full MP2 energy. The variational aspect of the MP2 ALMO-EDA is that energies (ii) through (v) are guaranteed to decrease, ensuring negative semidefinite energies for polarization, dispersion and CT. Counterpoise corrections[70,71] for basis set superposition error (BSSE) are included in those terms requiring it.

The magnitude of CT is increasingly underestimated in this procedure as the atomic orbital (AO) basis size is enlarged[62,72]. The reason is that polarization is captured before CT by a "greedy" variational algorithm where CT is supposed to be inhibited by the constraint of fragment-blocking the AO to MO transformation matrix (the ALMO approximation) and the correlation amplitudes. However, as the AO basis is increased in size, the ALMOs on one fragment gain the flexibility to slightly delocalize onto neighbor-

ing fragments, thereby capturing some CT within the polarization energy. This has been studied in detail previously[62,72] and methods have been introduced at the mean-field level which attain a stable and meaningful complete basis set limit value for CT[72,73]. While extending the MP2 ALMO-EDA to attain this same stability is desirable, using it in the original metastable form is an advantage in our present context, because it is important not to overestimate CT. We also note the fact that the CT contribution is counterpoise corrected to ensure that no BSSE is artificially ascribed to CT.

The most common way to apply an EDA traditionally has been by applying it to a single structure for each system (most commonly the minimum energy geometry) and decomposing that binding energy. However, for variational EDAs, an alternative method that has recently been proposed is the adiabatic EDA[74]. In it, instead of there being only a single structure, the system geometry is optimized at each successive level of the EDA: first the isolated molecules, then the system with only the frozen component allowed (this will include dispersion for dispersion corrected density functionals), next with both the frozen and polarization terms, and finally also allowing charge transfer, which means optimizing the overall energy. This way, the effect of each component can be seen on the geometry of the system and, for example, the charge transfer energy can be defined as the difference in energy between the optimum structures with and without charge transfer. This enables attribution of structural changes to the different physical contributions discussed above. In particular, we can assess the extent to which shortening of the XB distance in $R-X\cdots B$ is a consequence of CT. This type of analysis has previously been useful for determining that in the water dimer, CT is primarily responsible for the red shift in the proton donor OH stretch, and for more than 0.2 Å shortening of the hydrogen bond distance[75]. On the other hand, the linear geometry of the water dimer hydrogen bond was recovered without either polarization or CT[74].

3 Computational Methods

The energy decomposition analysis (EDA) methods used here are the SCF absolutely localized molecular orbitals (ALMO) EDA[63,73] and its MP2 extension[70,71] as described above. The calculations were performed in a development version of the Q-Chem quantum chemistry program package[76]. RI-MP2 was used for all calculations with the def2-TZVPP basis set using the rimp2-aug-cc-pVTZ auxiliary basis set. The def2-TZVPP set includes an ECP on the iodine atom. For MP2 ALMO-EDA calculations, H functions were removed from the auxiliary basis set because of code limitations. Energy differences resulting from this change were negligible. Counterpoise correction was used for all energies. All geometries were optimized with the same method and basis sets, with no constraints for the minima and with the I–Y^- distance constrained for the potential energy scan. As analytical gradient code is not yet available for the MP2 EDA, the adiabatic EDA[74] in this paper was done using Powell's method[77] on the internal coordinates, which does not require derivatives.

4 Results

In halogen bonds between the electron-pair acceptor molecule CX_3I and the donor ion Y^-, the trend in binding energy across different halogen substituents (X=F, Cl, Br, I) has been shown[16] to be opposite of that which is predicted by the σ-hole theory. Fluorine is the most electronegative atom, and so causes the highest potential in the σ-hole on the acceptor iodine atom. However, iodine is the substituent that leads to the strongest binding. This remains the case with several different halogen ions as the donor ($Y = F^-$, Cl^-, Br^-), as well as with other donors. The trend is also opposed to the permanent electrostatic one. CF_3I has a strong favorable charge-dipole interaction with the ion, while CI_4 has none. The different binding energies are shown in Figure 3.

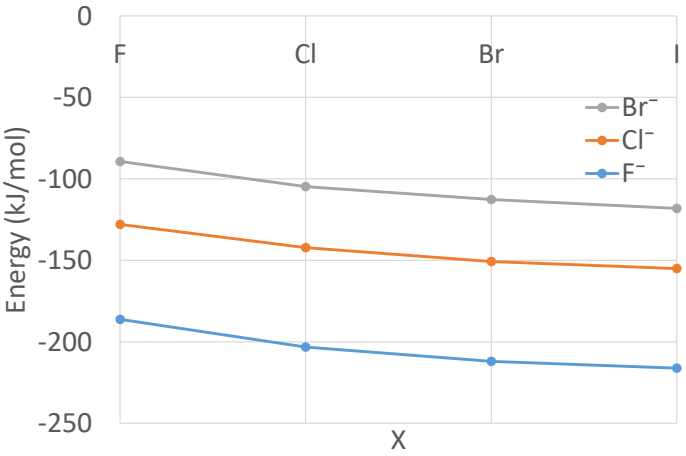

Fig. 3 Binding energy of $CX_3I\cdots Y^-$, for X=F, Cl, Br, I and Y=F, Cl, Br

This shows the previously discovered unexpected trend. Changing the donor ion changes the strength of the interaction, but leaves the overall trend nearly the same. Benchmark quality calculations confirm the trend. Complete basis set limit extrapolated MP2 numbers (with a two point aug-cc-pVQZ/aug-cc-PV5Z extrapolation) with a def2-QZVPPD ΔCCSD(T) correction gives a $CF_3I\cdots Cl^-$ binding energy of −116.1 kJ/mol and a $CI_4\cdots Cl^-$ binding energy of −145.2 kJ/mol, in fairly close agreement with the counterpoise corrected def2-TZVPP MP2 numbers. This raises the question of why the observed trend occurs, given that it contradicts the simple electrostatic prediction and a widely held theory. EDA will now be used to attempt to answer this question. First, the binding energies are decomposed into charge transfer in Figure 4 and frozen+polarization (which includes electrostatic and Pauli repulsion) in Figure 5. The dispersion interaction is similar enough in all cases to not affect the overall picture.

The decomposition attributes the substituent trend to increased charge transfer going down the periodic table. The electrostatic terms show the opposite trend, but makes less of a difference to the overall binding energy changes. This is at least partially because of the weakening dipole moment. On the other hand, most of the donor ion difference arises from electrostatics. One interesting point is that Cl^- complexes have weaker contributions from charge transfer than F^- complexes do, and have more repulsive frozen interactions. The first is odd because a Cl^- ion would

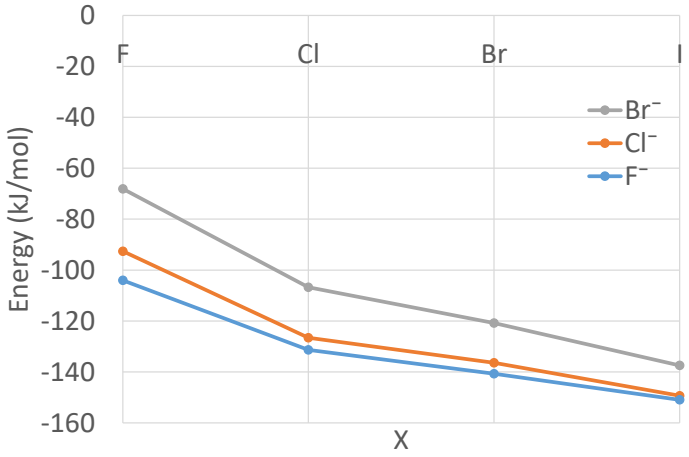

Fig. 4 Charge transfer energy of $CX_3I\cdots Y^-$, for X=F, Cl, Br, I and Y=F, Cl, Br

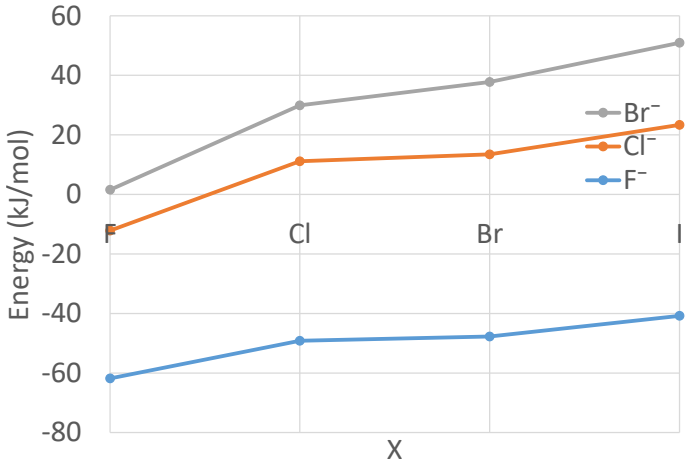

Fig. 5 Frozen + polarization energy of $CX_3I\cdots Y^-$, for X=F, Cl, Br, I and Y=F, Cl, Br

seem like a better electron donor than F^-. The second suggests the Pauli repulsion plays a role. As this must be resolved before examining other cases in detail, the EDA must be examined over other geometries.

The prior work applied the natural energy decomposition analysis[56,78] to these systems. The NEDA and ALMO EDA agree on the trend in charge transfer (though not the magnitude: NEDA gives CT energies triple that of ALMO EDA). Philosophical and definitional differences make the two methods problematic to compare directly, but the NEDA electrostatic trend is in the same direction as the charge transfer trend, while the ALMO EDA trend is opposite. This is largely due to different definitions of terms: NEDA includes permanent and induced electrostatics in a single electrostatic term and Pauli repulsion in separate core term, while ALMO EDA includes permanent electrostatics and Pauli repulsion in the frozen term and induced electrostatics in the polarization term. The larger magnitude of NEDA terms also makes direct comparison of the numbers difficult. However, the differences in behavior between permanent electrostatics, induced electrostatics, and Pauli repulsion can be explored in an ALMO EDA framework by looking at geometries beyond the minimum energy one.

One way of exploring more of the configuration space is to scan over the potential energy surface. This is done by constraining the $I\cdots Y^-$ separation to various distances and performing a geometry optimization at each point. From there, the binding energy can be decomposed for each optimized geometry. The results of this are shown in Figure 6(a) for $CI_4\cdots F^-$ and Figure 6(b) for $CI_4\cdots Cl^-$. The total energy curve also includes geometrical distortion, which is the energy difference between CI_4 and its minimum geometry energy. It is not included in any of the EDA components, but is too small to be visible in an interesting way on the graphs and so not shown.

As can be seen, CT is actually significantly greater for Cl^- than for F^- over the entire range observed. The difference is factor of two or three, confirming the common-sense intuition that Cl^- is a better donor for charge transfer. However, this was masked in the equilibrium structure EDA because of the different $I\cdots Y^-$ distances. The point in each curve that is not at a multiple of 0.5 Å is the minimum energy structure. Because the F^- minimum is over 0.5 Å closer, the CT when compared at the points of equilibrium is greater. The reason for the Cl^- being significantly farther out despite stronger charge transfer is the much greater Pauli repulsion. At 2.5 Å, the frozen term for Cl^- is over 200 kJ/mol more repulsive than for F^- (and off the plotted axes). Beyond 5 Å or so, the two frozen terms coincide within a few percent, as the electrostatics of both systems are a -1 ion interacting with the same dipole. The difference in the close range is due to the much greater Pauli repulsion resulting from the bulkier nature of the Cl^- ion. Most of the polarization difference is also due to Pauli repulsion, as it includes a correction to the frozen overestimation of it. In the long range, the two terms are similar because the main contribution is the charged induced dipole on the CI_4 molecule. Dispersion would also favor Cl^-, but the difference is not major. The fact that the equilibrium EDA obscured that Cl^- is a better electron donor than F^- shows the importance of EDA methods that look beyond a single structure.

An alternative approach is the adiabatic EDA[74]. The results are shown in table 1. In that framework, the binding energy difference comes at the (permanent and induced) electrostatic level. The relative energy of the polarized geometry is -105 kJ/mol for F^-, but only -54 kJ/mol for Cl^-. From there, charge transfer adds 98 kJ/mol for F^- and 72 kJ/mol for Cl^- when the systems are relaxed to their full minimum. The adiabatic EDA describes charge transfer as being stronger with F^-. However the two numbers are close, which is impressive for Cl^- because the interaction occurs at more than 0.5 Å greater distance. Looking at the adiabatic picture makes the importance of the greater distance clear because of the focus on the different geometries. Therefore, the three different ways of applying the EDA give three different pictures. At equilibrium only, the EDA shows CT and pol being weaker, and frz less repulsive, for Cl^- without providing much insight as to why that is. The potential energy scan EDA instead shows that CT at any given $I\cdots Y^-$ distance is significantly stronger for Cl^-, and the electrostatic parts of frz and pol roughly the same, but the much greater Pauli repulsion pushes the interaction to a larger distance where the interaction is weaker. And the adiabatic EDA says that the electrostatics alone make Cl^- bind

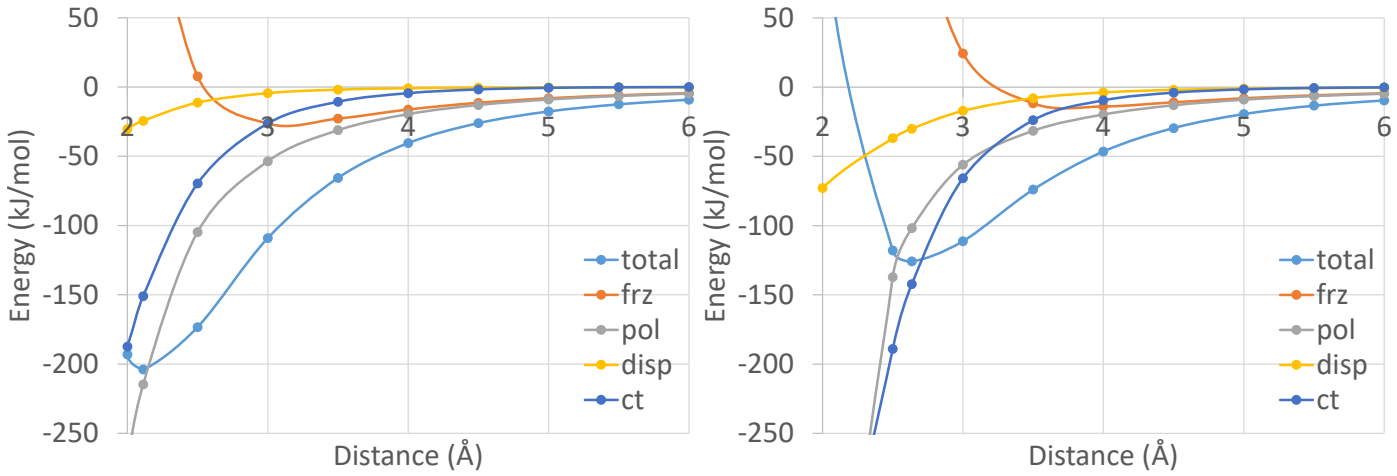

Fig. 6 (a) EDA for $CI_4\cdots F^-$ (b) EDA for $CI_4\cdots Cl^-$. The geometry is fully optimized at each $I\cdots Y^-$ distance

	$CI_4\cdots F^-$				$CI_4\cdots Cl^-$			
	sep	FRZ	POL	full	sep	FRZ	POL	full
E rel	0.000	−30.167	−105.670	−203.835	0.000	−19.675	−53.941	−125.837
GD	0.000	1.572	2.065	12.339	0.000	0.847	1.049	9.776
disp	-	−4.484	−11.151	−24.427	-	−6.650	−11.675	−30.047
frz	-	−27.255	4.917	173.846	-	−13.871	−2.547	138.480
pol	-	-	−101.501	−214.648	-	-	−40.768	−101.836
CT	-	-	-	−150.944	-	-	-	−142.210
r(C–X) (Å)	2.132	2.147	2.151	2.155	2.132	2.143	2.146	2.151
∠(X–C–X) (°)	109.47	111.02	111.24	111.15	109.47	110.60	110.77	110.74
r(C–I) (Å)	2.132	2.102	2.125	2.246	2.132	2.109	2.116	2.239
r(I···Y) (Å)	-	2.989	2.506	2.113	-	3.617	3.246	2.637
Dipole (D)	0.000	0.105	0.073	−0.176	0.000	0.056	0.055	−0.172

Table 1 Adiabatic EDA, where the column labels each correspond to the energy function used for geometry optimization: sep refers to infinitely separated fragments, FRZ is the frozen energy of the complex, POL also includes polarization, and full additionally includes CT. All energies in kJ/mol. E rel is the energy relative to infinite separation, GD is the geometric distortion energy, evaluated as the energy of the molecular fragment at its complex geometry minus that at its optimal geometry, and the dipole moment is for the molecular fragment, CI_4.

much weaker and farther than F^-, but that charge transfer plays a similarly sized role in both systems despite the larger distance. The latter two tackle the problem from different directions and provide complementary insights, but the first alone is not very enlightening.

With that settled, we can now turn back to the original question of the trend as substituents change. A similar analysis is necessary to tell which effects are genuinely weakened from CI_4 to CF_3I and which are lower merely due to the greater interaction distances. To start, the results of the relaxed potential energy scan EDA are shown in Figure 7(a) for $CF_3I\cdots F^-$ and Figure 7(b) for $CI_4\cdots F^-$ (repeated from Figure 6(a) for ease of comparison).

Comparing, we see that CI_4 has the greater charge transfer everywhere, by about 20 kJ/mol in the equilibrium range. This is about half the difference between the two binding energies. Much of the rest of the difference comes from the fact that CI_4 binds the fluoride closer, with equilibrium interaction distance of 2.11 Å, vs 2.20 Å for CF_3I. This happens because the greater CT is enough to overcome the frozen repulsion to a greater extent, even though it is more repulsive for CI_4. The large dipole moment of CF_3I shows up in the frozen term and is the main reason that it is less repulsive. However, the greater charge transfer is enough to compensate for the increase in the barrier, which is why the trend in these systems is opposite that predicted by electrostatics. While the EDA shows polarization as larger than charge transfer, in the short range the frozen and polarization terms should be considered together as they both describe the Pauli effect to some extent. Looking at the difference between the two polarization terms, we see that polarization is more favorable for CI_4 by about the same amount as charge transfer. This is because CI_4 is more polarizable than CF_3I. However, this alone would only be enough to make the interactions roughly equal in strength. Charge transfer is necessary to account for the CI_4 binding being significantly stronger.

The rest comes from the one body energies (once again, dispersion is essentially the same between the two systems). The CI_4 at equilibrium is 12 kJ/mol above its minimum geometry energy, while for CF_3I the number is 20 kJ/mol even though the interaction is weaker and therefore likely to have less of an effect on the geometry. This difference is significant on the scale of the difference between the interactions, suggesting that part of the stronger interaction with CI_4 may be because it is more easily

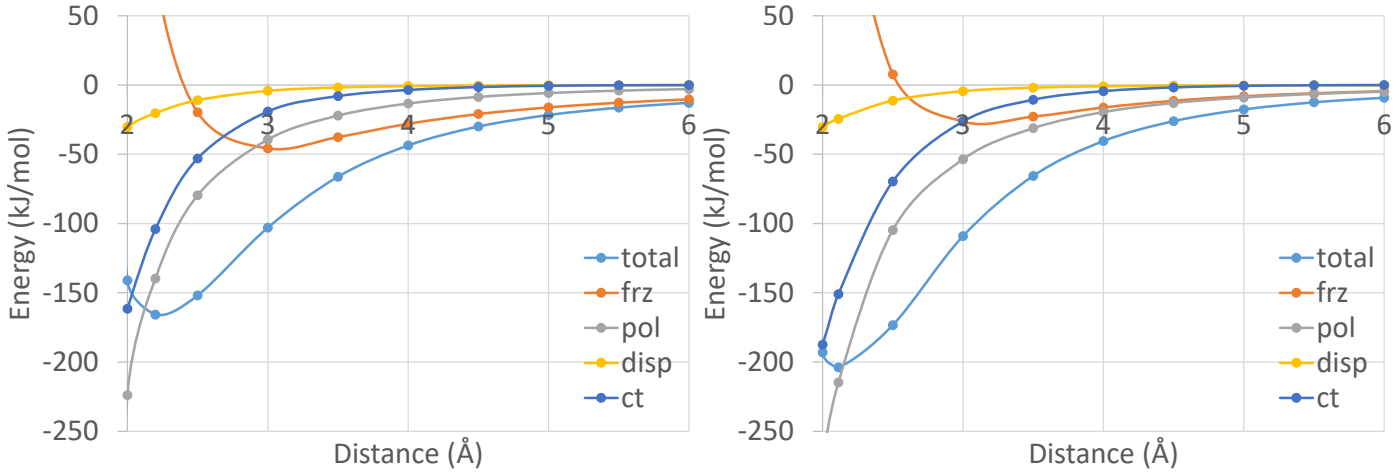

Fig. 7 (a) EDA for $CF_3I\cdots F^-$ (b) EDA for $CI_4\cdots F^-$

able to deform into the ideal geometry for charge transfer.

The same question can also be tackled with the adiabatic EDA, which can indicate how the different intermolecular forces influence the geometry of the system and allow the addition of each force to be considered separately. The $CX_3I\cdots Y^-$ system is simple enough that geometries can be specified by four parameters: C–X bond length, X–C–X bond angle, C–I bond length, and $I\cdots Y^-$ distance. The relative energies and geometry parameters for each system are shown in table 2. To match the procedure used with the DFT version of the adiabatic EDA, dispersion is included along with the frozen interaction.

The adiabatic EDA confirms that charge transfer is significantly stronger with iodine as the substituent atoms. While the polarized structures have roughly similar energies, CI_4 has 40 kJ/mol more gain in binding energy with the introduction of charge transfer than CF_3I. Most of the difference in polarization goes to overcoming the 15 kJ/mol that the frozen interaction favors CF_3I by. The adiabatic EDA confirms that polarization is only enough to make the two interactions roughly equal in strength, and charge transfer explains the large difference. Aside from the shrinking $I\cdots F$ distance, a notable trend is in the C–I bond length. The frozen geometries have a shorter bond than the isolated geometries, while the fully minimized geometries have a significantly longer one. As is typical, charge transfer into the acceptor bond weakens it and increases the length. On the other hand, a shorter C–I bond apparently leads to more favorable electrostatics, so the C–I bond length provides a measure of the relative importance of charge transfer and electrostatics. Interestingly, this leads to opposite trends in the dipole moment of the acceptor molecule. For CF_3I, dipole moment increases at every successive stage. With CI_4, this is not the case. The isolated molecule has no dipole by symmetry, but the presence of the fluoride ion causes the the molecule to shift to a slightly polar geometry at the frozen level. However, the polarized geometry reduces this, and the final geometry reverses it, leading to a moderate dipole moment away from the ion. This is further evidence that the halogen bond is not a primarily electrostatic phenomenon.

Incidentally, this means CI_4 has a long range favorable frozen interaction despite being nonpolar. It shows up in the potential energy scan because each point is an optimization with a constrained $I\cdots F$ distance. In the long range, where charge transfer is unimportant, the molecule can deform to be slightly polar and have a small favorable charge-dipole interaction with the ion. This supports the conclusion from the adiabatic EDA and explains it in terms of the dipole moment. Figure 8 shows the dipole moment for CX_3I at each point of the scan.

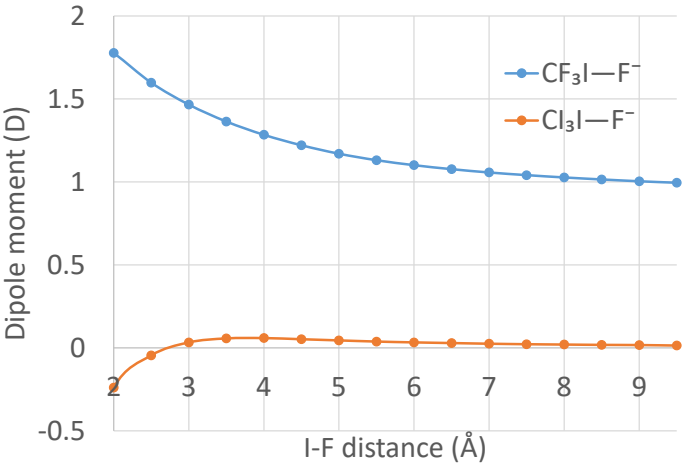

Fig. 8 CX_3I dipole moment at different constrained $I\cdots F$ distances

In the long range CI_4 does have a slight dipole moment for the reasons described above, and it increases until 4 Å. The CF_3I dipole also increases over this range. But while the CF_3I dipole continues to increase over the whole range, to nearly double its original value, the CI_4 reverses and actually becomes unfavorable in the interaction region. This mirrors the trend in the adiabatic EDA. The trends suggest that electrostatic effects are very important for the CF_3I geometries, as the presense of the ion pushes the dipole moment significantly higher, but that electrostatics and charge transfer have opposing roles in determining the CI_4 geometry and charge transfer wins out. One of the most important geometrical parameters is the C–I bond length, which is plotted at the different points of the scan in Figure 9. The dotted lines

	$CF_3I\cdots F^-$				$CI_4\cdots F^-$			
	sep	FRZ	POL	full	sep	FRZ	POL	full
E rel	0.000	−45.263	−100.768	−165.769	0.000	−30.167	−105.670	−203.835
GD	0.000	5.066	7.007	20.433	0.000	1.572	2.065	12.339
disp	-	−4.686	−9.599	−20.356	-	−4.484	−11.151	−24.427
frz	-	−45.643	−27.241	77.855	-	−27.255	4.917	173.846
pol	-	-	−70.935	−139.678	-	-	−101.501	−214.648
CT	-	-	-	−104.022	-	-	-	−150.944
r(C–X) (Å)	1.327	1.347	1.350	1.361	2.132	2.147	2.151	2.155
∠(X–C–X) (°)	110.57	112.67	112.98	113.78	109.47	111.02	111.24	111.15
r(C–I) (Å)	2.120	2.090	2.107	2.181	2.132	2.102	2.125	2.246
r(I···F) (Å)	-	2.935	2.564	2.198	-	2.989	2.506	2.113
Dipole (D)	0.907	1.497	1.561	1.699	0.000	0.105	0.073	−0.176

Table 2 Adiabatic EDA. All energies in kJ/mol. Dipole moment is of CX_3I. Numbers for $CI_4\cdots F^-$ repeated from table 1 for ease of comparison, all abbreviations and labels as defined in table 1.

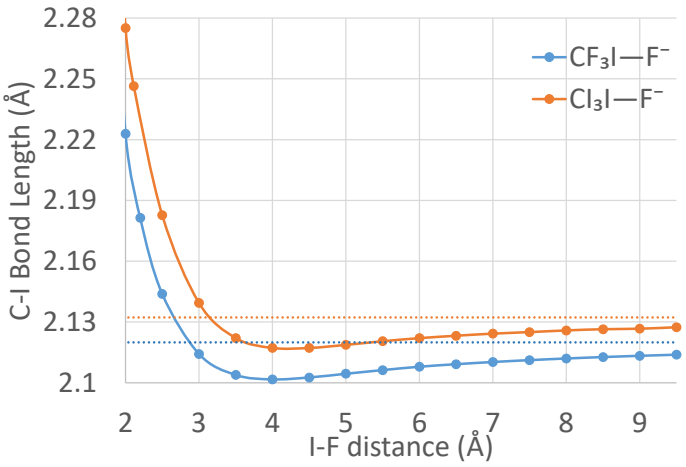

Fig. 9 Optimum C–I bond length at different constrained I···F distances

are bond lengths at the monomers' minimum energy geometries, which are the right asymptotes of the graphs. In both cases, the bonds are lengthened in the interaction region, though the effect is larger for CI_4 as expected from its greater charge transfer. But in CI_4 the bond lengthening is accompanied by an unfavorable dipole moment, while in CF_3I it is not. This suggests that, at least in CI_4, the C–I bond length can be used as a measure of the relative importance of electrostatics and charge transfer.

The conclusion supported by both EDA views is that electrostatics and charge transfer both play a role in the two examined halogen bonds. Electrostatics favors CF_3I while charge transfer favors CI_4 strongly enough that it is the significantly stronger interaction despite the electrostatics. Furthermore, the analysis seems to suggest that the CF_3I interaction is in some ways electrostatically dominated, with the geometry deforming to one favored by electrostatics. On the other hand, CI_4 seems charge transfer dominated, deforming to geometries against what is electrostatically favorable.

If those are examples of halogen bonds, one with good electrostatics but poor charge transfer and one with good charge transfer but poor electrostatics, it is useful to examine a case that is good on both counts. It is necessary to use a somewhat contrived example to accomplish this, but the nitro group is more electrostatic than fluorine and about as conducive to charge transfer as iodine. The molecule $C(NO_2)_3I$ forms an incredibly strong bond with F^- of about 260 kJ/mol, which is in the range of some covalent bonds. A potential energy scan of this system is shown in Figure 10.

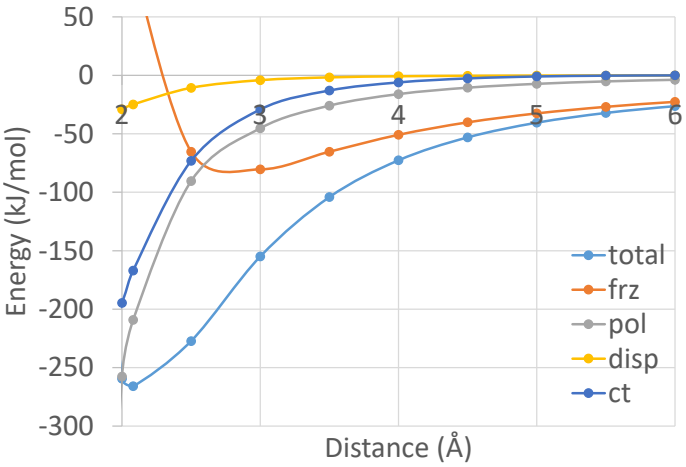

Fig. 10 EDA for $C(NO_2)_3I\cdots F^-$

The most noticeable difference on the graph is how much more favorable the frozen interaction is. At 2.5 Å, it is about 45 kJ/mol more favorable than even CF_3I, largely because of its huge dipole moment of 3.2 D (compared to 0.91 D). But unlike CF_3I which has a large increase in dipole moment as the ion gets closer, $C(NO_2)_3I$ shows more moderate behavior. The dipole moment increases slightly to a maximum of about 3.4 D at around 3 Å, but it drops back down to 3.3 D at equilibrium. This suggests that despite the dipole, the nature of the system is more similar to CI_4. Turning to charge transfer, we see behavior very similar to CI_4. In the range of 2–3 Å, it is about 10% stronger in $C(NO_2)_3I$. In the longer range, the charge transfer appears to be more slowly decaying, reaching twice the strength of CI_4 by 7 Å, but genuine charge transfer is difficult to distinguish from basis set superposition error at this distance. It seems that the properties of CI_4 that make it favorable to charge transfer are matched or slightly exceeded by $C(NO_2)_3I$. Finally (ignoring dispersion once again), there is

polarization. The value for $C(NO_2)_3I$ falls halfway in between CF_3I and CI_4 along the whole curve. While the polarization term contains some correction to Pauli repulsion in the short range, the differences between these three are electrostatic in nature, as all three systems have the same strength of Pauli repulsion. The charge induced dipole of the acceptor molecule should be much stronger than the dipole induced dipole on the F^- ion, so it is the main contributor to the polarization term. The polarizability of $C(NO_2)_3I$ is in between that of the other two acceptor molecules. That means these systems provide an example of a case where the trend in polarizability is different from the trend in charge transfer. Therefore, a picture of halogen bonding that replaces charge transfer with polarization would be unable to explain the strength of the $C(NO_2)_3I\cdots F^-$. With the dipole moment greater than in CF_3I, but the polarizability lower than in CI_4, a purely electrostatic model should not predict the extremely strong halogen bond observed.

The comparison between CF_3I, CI_4, and $C(NO_2)_3I$ shows that electrostatics and charge transfer act separately as forces in the halogen bond. They can be present in different strength in different systems, and either one alone would be insufficient to understanding the interaction. In CF_3I there is a favorable dipole moment, in CI_4 there is strong charge transfer, and in $C(NO_2)_3I$ there is both. It is important to examine more than just the equilibrium geometry when analyzing the interaction as the geometry is determined by the balance of frozen electrostatics, induced electrostatics, dispersion, and intermolecular charge transfer working against the wall of Pauli repulsion, so looking only at one geometry conflates the influences of all these forces. All of them are important for determining the overall interaction (though dispersion is very similar across the different systems, and so is not important for these comparisons), so each needs to be considered separately.

5 Conclusions

The σ-hole model has been claimed to fully account for halogen bonding,[27–35] although other studies have emphasized that charge transfer (CT) also plays a role in halogen bonding.[17–26] One possible piece of evidence for the role of CT is that σ-hole theory predicts the incorrect trend in strength of halogen bonds between CX_3I and either a halide ion or trimethylamine.[16] . It was suggested that this is because the σ-hole is a purely electrostatic descriptor, and some treatment of charge transfer is necessary to fully describe halogen bonding, as the two do not always coincide.

Using energy decomposition analysis, we have shown that charge transfer is indeed the differentiator between these various CX_3I and halide anion interactions. While the electrostatic trends are in the direction predicted by the σ-hole strength (and the dipole moment), the charge transfer trend is in the opposite direction and strong enough to overcome this deficit. The adiabatic EDA and EDA over the relaxed potential energy scan showed that looking only at the equilibrium is not enough by itself to resolve the relative strengths of the different forces, as the equilibrium geometry is determined by the balance between electrostatics, Pauli repulsion, charge transfer, and other effects, which all have different length scales. The analysis implies that the trend in binding energy is due to iodine substituents making the molecule a better acceptor for charge transfer. Comparison to another system showed that electrostatic favorability and charge transfer can vary separately. Because of this, it seems that no picture of the halogen bond can be complete without accounting for charge transfer and for the Lewis acid's suitability as an electron pair acceptor as well as its electrostatic properties. This has potential implications for the design of suitable descriptors for predicting the strength of halogen bonds.

6 Conflicts of interest

There are no conflicts to declare.

7 Acknowledgements

This work was supported by the Deutsche Forschungsgemeinschaft (DFG) in the context of the cluster of excellence RESOLV (EXC1069) and by CalSolv. MHG and JT acknowledge additional support from the U.S. National Science Foundation (Grants CHE-1665315 and CHE-136334).

References

1 P. Hobza, R. Zahradník and K. Müller-Dethlefs, *Collect. Czech. Chem. Commun.*, 2006, **71**, 443–531.
2 L. Gráfová, M. Pitoňák, J. Řezáč and P. Hobza, *J. Chem. Theory Comput.*, 2010, **6**, 2365–2376.
3 F. Guthrie, *J. Chem. Soc.*, 1863, **16**, 239–244.
4 J. P. M. Lommerse, A. J. Stone, R. Taylor and F. H. Allen, *J. Am. Chem. Soc.*, 1996, **118**, 3108–3116.
5 P. Metrangolo and G. Resnati, *Chem. Eur. J.*, 2001, **7**, 2511–2519.
6 P. Metrangolo, H. Neukirch, T. Pilati and G. Resnati, *Acc. Chem. Res.*, 2005, **38**, 386–395.
7 G. Cavallo, P. Metrangolo, R. Milani, T. Pilati, A. Priimagi, G. Resnati and G. Terraneo, *Chem. Rev.*, 2016, **116**, 2478–2601.
8 L. C. Gilday, S. W. Robinson, T. A. Barendt, M. J. Langton, B. R. Mullaney and P. D. Beer, *Chem. Rev.*, 2015, **115**, 7118–7195.
9 T. M. Beale, M. G. Chudzinski, M. G. Sarwar and M. S. Taylor, *Chem. Soc. Rev.*, 2013, **42**, 1667–1680.
10 S. H. Jungbauer, D. Bulfield, F. Kniep, C. W. Lehmann, E. Herdtweck and S. M. Huber, *J. Am. Chem. Soc.*, 2014, **136**, 16740–16743.
11 R. Wilcken, M. O. Zimmermann, A. Lange, A. C. Joerger and F. M. Boeckler, *J. Med. Chem.*, 2013, **56**, 1363–1388.
12 G. R. Desiraju, P. S. Ho, L. Kloo, A. C. Legon, R. Marquardt, P. Metrangolo, P. Politzer, G. Resnati and K. Rissanen, *Pure Appl. Chem.*, 2013, **85**, 1711–1713.
13 D. Bulfield and S. M. Huber, *Chem. Eur. J.*, 2016, **22**, 14434–14450.
14 O. Hassel, *Science*, 1970, **170**, 497–502.
15 A. E. Reed, F. Weinhold, R. Weiss and J. Macheleid, *J. Phys. Chem.*, 1985, **89**, 2688–2694.

16 S. M. Huber, E. Jimenez-Izal, J. M. Ugalde and I. Infante, *Chem. Commun.*, 2012, **48**, 7708.
17 L. P. Wolters and F. M. Bickelhaupt, *ChemistryOpen*, 2012, **1**, 96–105.
18 S. V. Rosokha, C. L. Stern and J. T. Ritzert, *Chem. Eur. J.*, 2013, **19**, 8774–8788.
19 B. Pinter, N. Nagels, W. A. Herrebout and F. De, Proft, *Chem. Eur. J.*, 2013, **19**, 518–529.
20 S. M. Huber, J. D. Scanlon, E. Jimenez-Izal, J. M. Ugalde and I. Infante, *Phys. Chem. Chem. Phys.*, 2013, **15**, 10350–10357.
21 L. P. Wolters, P. Schyman, M. J. Pavan, W. L. Jorgensen, F. M. Bickelhaupt and S. Kozuch, *WIREs Comput. Mol. Sci.*, 2014, **4**, 523–540.
22 C. Wang, D. Danovich, Y. Mo and S. Shaik, *J. Chem. Theory Comput.*, 2014, **10**, 3726–3737.
23 L. P. Wolters, N. W. G. Smits and C. Fonseca Guerra, *Phys. Chem. Chem. Phys.*, 2015, **17**, 1585–1592.
24 S. W. Robinson, C. L. Mustoe, N. G. White, A. Brown, A. L. Thompson, P. Kennepohl and P. Beer, *J. Am. Chem. Soc.*, 2015, **137**, 499–507.
25 V. Oliveira, E. Kraka and D. Cremer, *Phys. Chem. Chem. Phys.*, 2016, **18**, 33031–33046.
26 V. Oliveira, E. Kraka and D. Cremer, *Inorg. Chem.*, 2017, **56**, 488–502.
27 T. Clark, M. Hennemann, J. S. Murray and P. Politzer, *J. Mol. Model.*, 2006, **13**, 291–296.
28 P. Politzer, P. Lane, M. C. Concha, Y. Ma and J. S. Murray, *J. Mol. Model.*, 2006, **13**, 305–311.
29 P. Politzer, J. S. Murray and T. Clark, *Phys. Chem. Chem. Phys.*, 2010, **12**, 7748.
30 P. Politzer, J. S. Murray and T. Clark, *Phys. Chem. Chem. Phys.*, 2013, **15**, 11178.
31 P. Politzer and J. S. Murray, *ChemPhysChem*, 2013, **14**, 278–294.
32 M. Kolar, J. Hostas and P. Hobza, *Phys. Chem. Chem. Phys.*, 2014, **16**, 9987–9996.
33 P. Politzer, J. S. Murray and T. Clark, *J. Mol. Model.*, 2015, **21**, 52.
34 T. Clark, P. Politzer and J. S. Murray, *WIREs Comput. Mol. Sci.*, 2015, **5**, 169–177.
35 M. H. Kolar and P. Hobza, *Chem. Rev.*, 2016, **116**, 5155–5187.
36 K. E. Riley and P. Hobza, *Phys. Chem. Chem. Phys.*, 2013, **15**, 17742–17751.
37 A. J. Stone, *J. Am. Chem. Soc.*, 2013, **135**, 7005–7009.
38 S. J. Grabowski, *Phys. Chem. Chem. Phys.*, 2013, **15**, 7249.
39 K. Hermansson, *J. Phys. Chem. A*, 2002, **106**, 4695–4702.
40 W. Qian and S. Krimm, *J. Phys. Chem. A*, 2002, **106**, 6628–6636.
41 J. S. Murray, M. C. Concha, P. Lane, P. Hobza and P. Politzer, *J. Mol. Model.*, 2008, **14**, 699–704.
42 M. Hennemann, J. S. Murray, P. Politzer, K. E. Riley and T. Clark, *J. Mol. Model.*, 2011, **18**, 2461–2469.
43 K. E. Riley, J. S. Murray, P. Politzer, M. C. Concha and P. Hobza, *J. Chem. Theory Comput.*, 2009, **5**, 155–163.
44 Z. P. Shields, J. S. Murray and P. Politzer, *Int. J. Quantum Chem.*, 2010, **110**, 2823–2832.
45 K. E. Riley, J. S. Murray, J. Fanfrlík, J. Řezáč, R. J. Solá, M. C. Concha, F. M. Ramos and P. Politzer, *J. Mol. Model.*, 2011, **17**, 3309–3318.
46 R. Khaliullin, A. Bell and M. Head-Gordon, *J. Chem. Phys.*, 2008, **128**, 184112.
47 A. E. Reed, L. A. Curtiss and F. Weinhold, *Chem. Rev.*, 1988, **88**, 899–926.
48 B. Jeziorski, R. Moszynski and K. Szalewicz, *Chem. Rev.*, 1994, **94**, 1887–1930.
49 F. Bickelhaupt and E. Baerends, *Rev. Comput. Chem.*, 2000, **15**, 1–86.
50 M. von Hopffgarten and G. Frenking, *WIRES Comput. Mol. Sci.*, 2012, **2**, 43–62.
51 M. J. S. Phipps, T. Fox, C. S. Tautermann and C.-K. Skylaris, *Chem. Soc. Rev.*, 2015, **44**, 3177–3211.
52 E. Pastorczak and C. Corminboeuf, *J. Chem. Phys.*, 2017, **146**, 120901.
53 F. Weinhold, C. R. Landis and E. D. Glendening, *Int. Rev. Phys. Chem.*, 2016, **35**, 399–440.
54 R. Z. Khaliullin, A. T. Bell and M. Head-Gordon, *Chem. Eur. J.*, 2009, **15**, 851–855.
55 A. J. Stone, *J. Phys. Chem. A*, 2017, **121**, 1531–1534.
56 E. D. Glendening, *J. Phys. Chem. A*, 2005, **109**, 11936–11940.
57 F. Weinhold, *Adv. Protein Chem.*, 2006, **72**, 121.
58 F. Weinhold and R. A. Klein, *Chem. Educ. Res. Pract.*, 2014, **15**, 276–285.
59 F. Weinhold and R. A. Klein, *Angew. Chem. Int. Ed.*, 2014, **53**, 11214–11217.
60 F. Weinhold and R. A. Klein, *Mol. Phys.*, 2012, **110**, 565–579.
61 K. U. Lao and J. M. Herbert, *J. Chem. Theor. Comput.*, 2016, **12**, 2569–2582.
62 R. J. Azar, P. R. Horn, E. J. Sundstrom and M. Head-Gordon, *J. Chem. Phys.*, 2013, **138**, 084102.
63 R. Z. Khaliullin, E. A. Cobar, R. C. Lochan, A. T. Bell and M. Head-Gordon, *J. Phys. Chem. A*, 2007, **111**, 8753–8765.
64 R. Z. Khaliullin, M. Head-Gordon and A. T. Bell, *J. Chem. Phys.*, 2006, **124**, 204105.
65 P. R. Horn, E. J. Sundstrom, T. A. Baker and M. Head-Gordon, *J. Chem. Phys.*, 2013, **138**, 134119.
66 K. Kitaura and K. Morokuma, *Int. J. Quant. Chem.*, 1976, **10**, 325–340.
67 T. Ziegler and A. Rauk, *Theor. Chim. Acta*, 1977, **46**, 1–10.
68 Y. R. Mo, J. L. Gao and S. D. Peyerimhoff, *J. Chem. Phys.*, 2000, **112**, 5530–5538.
69 Y. R. Mo, P. Bao and J. L. Gao, *Phys. Chem. Chem. Phys.*, 2011, **13**, 6760–6775.
70 J. Thirman and M. Head-Gordon, *J. Chem. Phys.*, 2015, **143**, 084124.
71 J. Thirman and M. Head-Gordon, *J. Phys. Chem. A*, 2017, **121**, 717–728.

72 P. R. Horn and M. Head-Gordon, *J. Chem. Phys.*, 2015, **143**, 114111.

73 P. R. Horn, E. J. Sundstrom, T. A. Baker and M. Head-Gordon, *J. Chem. Phys.*, 2013, **138**, 134119.

74 Y. Mao, P. R. Horn and M. Head-Gordon, *Phys. Chem. Chem. Phys.*, 2017, **19**, 5944–5958.

75 E. Ramos-Cordoba, D. S. Lambrecht and M. Head-Gordon, *Faraday Disc.*, 2011, **150**, 345–362.

76 Y. Shao, Z. Gan, E. Epifanovsky, A. T. B. Gilbert, M. Wormit, J. Kussmann, A. W. Lange, A. Behn, J. Deng, X. Feng, D. Ghosh, M. Goldey, P. R. Horn, L. D. Jacobson, I. Kaliman, R. Z. Khaliullin, T. Kús, A. Landau, J. Liu, E. I. Proynov, Y. M. Rhee, R. M. Richard, M. A. Rohrdanz, R. P. Steele, E. J. Sundstrom, H. L. Woodcock III, P. M. Zimmerman, D. Zuev, B. Albrecht, E. Alguire, B. Austin, G. J. O. Beran, Y. A. Bernard, E. Berquist, K. Brandhorst, K. B. Bravaya, S. T. Brown, D. Casanova, C.-M. Chang, Y. Chen, S. H. Chien, K. D. Closser, D. L. Crittenden, M. Diedenhofen, R. A. DiStasio Jr., H. Dop, A. D. Dutoi, R. G. Edgar, S. Fatehi, L. Fusti-Molnar, A. Ghysels, A. Golubeva-Zadorozhnaya, J. Gomes, M. W. D. Hanson-Heine, P. H. P. Harbach, A. W. Hauser, E. G. Hohenstein, Z. C. Holden, T.-C. Jagau, H. Ji, B. Kaduk, K. Khistyaev, J. Kim, J. Kim, R. A. King, P. Klunzinger, D. Kosenkov, T. Kowalczyk, C. M. Krauter, K. U. Lao, A. Laurent, K. V. Lawler, S. V. Levchenko, C. Y. Lin, F. Liu, E. Livshits, R. C. Lochan, A. Luenser, P. Manohar, S. F. Manzer, S.-P. Mao, N. Mardirossian, A. V. Marenich, S. A. Maurer, N. J. Mayhall, C. M. Oana, R. Olivares-Amaya, D. P. O'Neill, J. A. Parkhill, T. M. Perrine, R. Peverati, P. A. Pieniazek, A. Prociuk, D. R. Rehn, E. Rosta, N. J. Russ, N. Sergueev, S. M. Sharada, S. Sharmaa, D. W. Small, A. Sodt, T. Stein, D. Stück, Y.-C. Su, A. J. W. Thom, T. Tsuchimochi, L. Vogt, O. Vydrov, T. Wang, M. A. Watson, J. Wenzel, A. White, C. F. Williams, V. Vanovschi, S. Yeganeh, S. R. Yost, Z.-Q. You, I. Y. Zhang, X. Zhang, Y. Zhou, B. R. Brooks, G. K. L. Chan, D. M. Chipman, C. J. Cramer, W. A. Goddard III, M. S. Gordon, W. J. Hehre, A. Klamt, H. F. Schaefer III, M. W. Schmidt, C. D. Sherrill, D. G. Truhlar, A. Warshel, X. Xua, A. Aspuru-Guzik, R. Baer, A. T. Bell, N. A. Besley, J.-D. Chai, A. Dreuw, B. D. Dunietz, T. R. Furlani, S. R. Gwaltney, C.-P. Hsu, Y. Jung, J. Kong, D. S. Lambrecht, W. Liang, C. Ochsenfeld, V. A. Rassolov, L. V. Slipchenko, J. E. Subotnik, T. Van Voorhis, J. M. Herbert, A. I. Krylov, P. M. W. Gill and M. Head-Gordon, *Mol. Phys.*, 2015, **113**, 184–215.

77 M. J. D. Powell, *Comput. J.*, 1964, **7**, 155–162.

78 E. D. Glendening and A. Streitwieser, *J. Chem. Phys.*, 1994, **100**, 2900.